

## On Richtmyer–Meshkov instability in dilute gas-particle mixtures

Satoshi Ukai,<sup>a)</sup> Kaushik Balakrishnan,<sup>b)</sup> and Suresh Menon<sup>c)</sup>  
*Georgia Institute of Technology, Atlanta, Georgia 30332-0150, USA*

(Received 8 July 2010; accepted 6 October 2010; published online 29 October 2010)

Richtmyer–Meshkov instability (RMI) in gas-particle mixtures is investigated both numerically and analytically. The linear amplitude growth rate for a RMI in a two-phase mixture is derived by using a dusty gas formulation for small Stokes number ( $St \ll 1.0$ ), and it is shown that the problem can be characterized by mass loading and  $St$ . The model predictions are compared with numerical results under two conditions, i.e., a shock wave hitting (1) a perturbed species interface of air and SF<sub>6</sub> surrounded by uniformly distributed particles, and (2) a perturbed shape particle cloud in uniform air. In the first case, the interaction between the instability of the species perturbation and the particles is investigated. The multiphase growth model accurately predicts the growth rates when  $St \ll 1.0$ , and the amplitude growth normalized by the two-phase RMI velocity shows good agreement with the single-phase RMI growth rate as well. It is also shown that the two-phase model results are in accordance with the growth rates obtained from the simulations even for cases corresponding to  $St \approx 10$ . However, for  $St \gg 10$ , particles do not follow the RMI motion, and the RMI growth rate agrees with the original Richtmyer’s model [R. D. Richtmyer, “Taylor instability in shock acceleration of compressible fluids,” *Commun. Pure Appl. Math.* **13**, 297 (1960)]. Preferential concentration of particles are observed around the RMI roll-ups at late times when  $St$  is of order unity, whereas when  $St \ll 1.0$ , the particles respond rapidly to the flow, causing them to distribute within the roll-ups. In the second problem, the two-phase RMI growth model is extended to study whether a perturbed dusty gas front shows RMI-like growth due to the impact of a shock wave. When  $St \ll 1.0$ , good agreement with the multiphase model is again seen. Moreover, the normalized growth rates are very close to the single-phase RMI growth rates even at late times, which suggest that the two-phase growth model is applicable to this type of perturbed shape particle clouds as well. However, when  $St$  is close to unity or larger ( $St > 1.0$ ), the particles do not experience impulsive acceleration but rather a continuous one, which results in exponential growth rates as seen in a Rayleigh–Taylor instability. © 2010 American Institute of Physics.  
 [doi:[10.1063/1.3507318](https://doi.org/10.1063/1.3507318)]

### I. INTRODUCTION

Richtmyer–Meshkov instability (RMI) is caused by an impulsive acceleration of a perturbed interface between two media of different densities.<sup>1,2</sup> A primary interest in RMI study is to understand the amplitude growth rate of the perturbation, since it is a direct measure of the mixing between the two fluids. RMI growth can be identified by a bubble and a spike; a bubble is defined as the region where the lighter fluid penetrates into the heavier fluid, and similarly, a spike is the region where the heavier fluid penetrates into the lighter fluid. An amplitude  $a$  is defined as one-half of the distance between the bubble and the spike front.

Numerous theoretical/empirical growth models of single-mode perturbation have been proposed in the past and have been validated against experimental and numerical studies.<sup>3–6</sup> However, RMI occurring in natural and engineering environments are generally more complex. Therefore, many studies investigated RMI with more complex interface

conditions such as a multimode interface,<sup>7</sup> with a reshock,<sup>8,9</sup> in cylindrical geometries,<sup>10</sup> and in spherical explosions.<sup>11</sup> However, most of these past studies have focused on single-phase flow. RMI effects in two-phase flows are also important for various applications such as explosions with reactive metal particles,<sup>11</sup> chondrules concentration in a nebula,<sup>12</sup> and possibly other multiphase systems involving shock waves.

In general, particles in a flow field are known to affect the instability of the gas-phase. For example, it has been shown that particles modify the Orr–Sommerfeld equation and stabilize or destabilize the transition to turbulence depending on the particle size.<sup>13</sup> In another study, it was shown that the amplitude growth rate of two-phase Kelvin–Helmholtz instability<sup>14</sup> (KHI) was reduced due to particles in the vicinity of the interface. On the other hand, it appears that the interaction of a RMI with particle clouds has never been studied to the best of the authors’ knowledge. Past studies analyzed the two-phase fluid instability by performing a linear perturbation analysis on the dusty gas formulation<sup>13–15</sup> that assumes that the particle shapes and sizes are uniform, and the particle motions can be described by the Eulerian coordinate. Here, the dusty gas formulation is employed to establish a linear growth model of two-phase RMI similar to Richtmyer’s model.<sup>1</sup> However, since the model is explored

<sup>a)</sup>Present address: Institut für Technische Verbrennung, Universität Stuttgart, 70569 Stuttgart, Germany.

<sup>b)</sup>Present address: Computing Sciences, Lawrence Berkeley National Laboratory, 1 Cyclotron Road, Berkeley, CA 94720, USA.

<sup>c)</sup>Electronic mail: suresh.menon@aerospace.gatech.edu.

only in a certain regime due to the nature of the governing equations of the perturbation method and the assumptions made, numerical simulations are performed with different particle sizes and mass loadings of particles to study a wider range of initial conditions.

The dusty gas formulation<sup>13</sup> assumes that a particle cloud itself can be treated as a different gas, a region filled with particles can be considered to have a larger density, and the RMI growth model can be explored under certain conditions. There are various studies of deformation of particle clouds by shocks with different shapes of particle clustering,<sup>16–18</sup> but none of them have been analyzed in terms of RMI. For example, Ota *et al.*<sup>19</sup> observed the deformation of a half-height dense gas caused by a shock wave, and Kiselev *et al.*<sup>17</sup> performed numerical simulations with a similar setup but having particle clouds instead of a heavy gas. Their results showed qualitatively that particle dispersion shapes are very similar to the deformation of a dense gas. Other past numerical studies<sup>20,21</sup> investigated clouds of heavy particles falling into a light fluid, and reported the formation of structures similar to the Rayleigh–Taylor instability (RTI). In the present study, the shock accelerated perturbed particle cloud is analyzed by using the two-phase RMI growth model to examine whether the amplitude growth follows RMI-type growth rates.

Two different types of two-phase RMI are analyzed in the present work. The first type involves the impulsive acceleration of a perturbed species interface of air/SF<sub>6</sub> surrounded by a uniformly distributed cloud of particles. The second type of RMI study considered here is the shock wave induced dispersion of a particle cloud with a perturbed shape within a uniform gas. Numerical simulations for a range of conditions are performed and compared to a new theoretical model prediction.

This paper is organized as follows. The governing equations for the gas and solid phases are presented in Sec. II. The growth model of two-phase RMI is formulated in Sec. III. The results of RMI surrounded by the particles and the RMI with the perturbed shape particle clouds are discussed in Sec. IV. Finally, the conclusions drawn from this study are presented in Sec. V.

## II. SIMULATION METHODOLOGY

### A. Gas phase

The compressible Navier–Stokes equations for multispecies and multiphase flows under the dilute limit (negligible solid volume fraction) are<sup>11</sup>

$$\frac{\partial \rho}{\partial t} + \frac{\partial \rho u_i}{\partial x_i} = \dot{\rho}_p, \quad (1)$$

$$\frac{\partial \rho u_i}{\partial t} + \frac{\partial}{\partial x_j} (\rho u_i u_j + p \delta_{ij} - \tau_{ij}) = \dot{F}_{p,i}, \quad (2)$$

$$\frac{\partial \rho E}{\partial t} + \frac{\partial}{\partial x_i} [(\rho E + p)u_i + q_i - u_j \tau_{ij}] = \dot{Q}_p + \dot{W}_p, \quad (3)$$

$$\frac{\partial \rho Y_k}{\partial t} + \frac{\partial}{\partial x_i} (\rho Y_k u_i + J_{i,k}) = \dot{S}_{p,k} \quad k = 1, \dots, N_s. \quad (4)$$

Here,  $\rho$  is the density,  $(u_i)_{i=1,2,3}$  is the velocity vector in Cartesian coordinates,  $p$  is the pressure,  $E$  is the total energy,  $Y_k$  is the mass fraction for species  $k$ ,  $\tau_{ij}$  is shear stress tensor,  $q_i$  is the rate of heat transfer,  $J_{i,k}$  is the diffusion flux, and  $N_s$  is the total number of species in the flow.  $\dot{\rho}_p$ ,  $\dot{F}_{p,i}$ ,  $\dot{Q}_{p,i}$ ,  $\dot{W}_{p,i}$ , and  $\dot{S}_{p,k}$  are the source terms of mass, momentum, heat, work, and species due to the presence of particles. The current study assumes that the particle loading is dilute, so that volume occupied by particles is considered to be negligible. Also in this study, only momentum exchange is considered, hence,  $\dot{F}_{p,i} \neq 0$ . The pressure is computed from the equation of state for a calorically perfect gas as  $p = \rho RT$ , where  $T$  is the temperature and the mixture averaged gas constant is obtained as  $R = \sum_{k=1}^{N_s} Y_k (R_u / MW_k)$ , where  $R_u$  is the universal gas constant and  $MW_k$  is the molecular weight of the  $k$ th species.

Since RMI involves large gradients at the shock front and the species interface, as well as smooth regions such as shear layers, this study uses a hybrid scheme<sup>22,23</sup> that switches the flow solver depending on the local flow conditions, and the scheme has been validated for various engineering flows involving shocks, turbulence,<sup>22–24</sup> and multiphase flows.<sup>11,25</sup> The hybrid scheme uses a fourth-order central scheme within smooth regions and reverts to a flux difference splitting method in regions of strong gradients. The monotone upstream-centered schemes for conservation laws approach is used to reconstruct the flow variables at intercell interfaces, and a hybrid Riemann solver, Harten Lax van Leer Contact/Einfeldt (HLLC/E), is applied to obtain the intercell fluxes.<sup>22</sup> Details of the numerical schemes are available elsewhere.<sup>22–24</sup>

### B. Particle phase

This study utilizes the Lagrangian tracking method that computes the velocity and location of each point-particle. This approach has been used in the past for particle tracking and is well established.<sup>26</sup> The particle trajectories are computed by solving the following governing equations:

$$\frac{d\mathbf{x}_p}{dt} = \mathbf{v}, \quad (5)$$

$$m \frac{d\mathbf{v}}{dt} = \frac{\pi}{2} r_p^2 C_D \rho |\mathbf{u} - \mathbf{v}| (\mathbf{u} - \mathbf{v}), \quad (6)$$

where  $\mathbf{x}_p$  is the position of the particle,  $\mathbf{u}$  is the local velocity of the gas at the location of the particle,  $\mathbf{v}$  is the velocity of the particle,  $m$  is the particle mass,  $r$  is the particle radius, and  $C_D$  is the drag coefficient. The drag coefficient is generally expressed as a function of the particle Reynolds number,  $Re_d = \frac{2r_p \rho |\mathbf{u} - \mathbf{v}|}{\mu}$ , where  $\mu$  is the dynamic viscosity of the gas. Equation (6) typically contains other terms on the right hand side to include the effect of pressure gradient, the Basset term, the Saffman lift, and the Magnus lift.<sup>27</sup> For this dilute study, all these effects are neglected as a first approximation.

Assuming the particles are spherical, the drag coefficient  $C_D$  is obtained from the empirical relations<sup>26</sup> as

$$C_D = \begin{cases} \frac{24}{Re_d} \left( 1 + \frac{1}{6} Re_d^{2/3} \right) & Re_d < 1000, \\ 0.424 & Re_d > 1000. \end{cases} \quad (7)$$

It is shown that heat transfer between the fluid and the particles can affect shock-particle interactions.<sup>28</sup> However, heat transfer is neglected in the present study as also done in previous instability analysis,<sup>13,14</sup> but will be investigated in a latter study. The parcel method<sup>29</sup> is used to approximate particle clouds, where a parcel consists of a group of particles that carries the same properties. This approach significantly reduces the computational memory requirements; detailed explanation of the parcel method is available elsewhere.<sup>29,25</sup> A fourth-order Runge–Kutta method is used to integrate Eqs. (5) and (6) in time.

### III. AMPLITUDE GROWTH MODEL FOR MULTIPHASE RMI

Richtmyer<sup>1</sup> originally derived the linear growth model of RMI by applying an impulsive acceleration to the growth model of the RTI derived from a linear perturbation analysis<sup>30</sup> and obtained the following linear growth with time ( $t$ ):

$$a(t) = v_0 t + a_0, \quad (8)$$

where  $a$  is the instantaneous amplitude,  $a_0$  is the initial amplitude,  $v_0$  is the Richtmyer velocity defined as  $v_0 = ka_0 A \Delta V$ ,  $k$  is the wavenumber given as  $k = 2\pi/\lambda$ ,  $\lambda$  is the wavelength,  $A$  is the Atwood number defined as  $A = (\rho_2 - \rho_1)/(\rho_2 + \rho_1)$ ,  $\rho_2$  and  $\rho_1$  are the density of the heavy and the light fluid, respectively, and  $\Delta V$  is the change in the speed of the interface by an incident shock. However, the impulsive model is only applicable at early times where  $ka < 0.3$ .<sup>3</sup>

A growth model for two-phase RMI is obtained by following a similar approach but by employing the dusty gas formulation<sup>13</sup> that assumes the volume fraction of particles are very small, and that the interaction between particles is neglected. The linear perturbation analysis is first used to obtain the growth rate of two-phase RTI following a past KHI study,<sup>14</sup> and then the two-phase RMI growth rates are evaluated by the impulsive method.<sup>1</sup>

The dusty gas equations for a mixture of gas and a pseudofluid of small particles can be written as<sup>13</sup>

$$\rho \left[ \frac{\partial \mathbf{u}}{\partial t} + (\mathbf{u} \cdot \nabla) \mathbf{u} \right] = -\nabla p + \mu \nabla^2 \mathbf{u} + \kappa N (\mathbf{v} - \mathbf{u}) + \rho g \nabla z, \quad (9)$$

$$\nabla \cdot \mathbf{u} = 0, \quad (10)$$

$$mN \left[ \frac{\partial \mathbf{v}}{\partial t} + (\mathbf{v} \cdot \nabla) \mathbf{v} \right] = \kappa N (\mathbf{u} - \mathbf{v}) + mg \nabla (Nz), \quad (11)$$

$$\frac{\partial N}{\partial t} + \nabla \cdot N \mathbf{v} = 0, \quad (12)$$

where  $\mathbf{u}$  is the gas velocity,  $\mathbf{v}$  is the velocity of the particles,  $p$  is the gas pressure,  $\mu$  is the gas viscosity,  $\rho$  is the gas density,  $\kappa$  is the drag term,  $N$  is the number density of the particles,  $m$  is the mass of the particle,  $z$  is the height, and  $g$  is the driving acceleration. Assuming the particles are spherical,  $\kappa = 6\pi r_p \mu$  is used from Stokes' law,<sup>13</sup> where  $r_p$  is the radius of particle. Note that the drag law used for the theoretical analysis is simpler than that used in the numerical simulation [Eq. (7)] in order to maintain linearity of the theoretical formulation.

Also, the pseudofluid formulation is incompressible since it is assumed that once the shock wave passes the interface, the flow is incompressible, as also assumed by Richtmyer.<sup>1</sup> The equations are linearized by considering a small perturbation as follows

$$\mathbf{u} = \mathbf{U}_0 + \mathbf{u}', \mathbf{v} = \mathbf{U}_0 + \mathbf{v}', N = N_0 + N', \quad (13)$$

$$p = p_0 + p', z = z_0 + a.$$

Here  $\mathbf{U}_0$ ,  $N_0$ ,  $p_0$ , and  $z_0$  are, respectively, the mean velocity, the number density, the pressure, and the particle position. Note that  $\mathbf{U}_0$  is the mean velocity only in the  $x$ -direction, and the mean particle velocity is equated to the gas velocity,  $\mathbf{U}_0$  as also assumed in the original papers.<sup>13,14</sup> Also,  $z_0$  is the reference height chosen to be zero.  $\mathbf{u}'$ ,  $\mathbf{v}'$ ,  $N'$ , and  $p'$  are the corresponding fluctuation of each parameter, and  $a$  is the amplitude of the perturbation. Each disturbance is represented by a wave of the form in two-dimensional<sup>13,14</sup> (2D)

$$\begin{aligned} & [\mathbf{u}'(x, z, t), \mathbf{v}'(x, z, t), N'(x, z, t), p'(x, z, t), a(x, t)] \\ & = [\hat{\mathbf{u}}(z), \hat{\mathbf{v}}(z), \hat{N}(z), \hat{p}(z), \hat{a}] e^{ik(x-ct)}. \end{aligned} \quad (14)$$

Here, all variables with hat ( $\hat{\cdot}$ ) are the complex amplitudes,  $k$  is the streamwise wavenumber, and  $c$  is the complex phase velocity. Assuming small perturbations and inviscid conditions,<sup>30</sup> Eqs. (9) and (11) are linearized as follows

$$ik(U_0 - c)\hat{\mathbf{u}} = -ik\hat{p}/\rho + s(\hat{\mathbf{v}} - \hat{\mathbf{u}}) + ikg\hat{a}, \quad (15)$$

$$ik(U_0 - c)\hat{\mathbf{v}} = (\hat{\mathbf{u}} - \hat{\mathbf{v}})/\tau + ikg\hat{a}. \quad (16)$$

Here,  $s = \kappa N_0/\rho$  and  $\tau = m/\kappa$ . Note that  $s$  has units of frequency and  $\tau$  is the particle response time with units of time.

In Eq. (17) below,  $\hat{p}$  is obtained by a function of  $\hat{\mathbf{u}}$  by combining Eqs. (15) and (16) (Refs. 13)

$$\begin{aligned} (U_0 - c) \left[ 1 + \frac{\tau s}{1 + ik\tau(U_0 - c)} \right] \hat{\mathbf{u}} \\ = -\hat{p}/\rho + \left[ 1 + \frac{\tau s}{1 + ik\tau(U_0 - c)} \right] g\hat{a}. \end{aligned} \quad (17)$$

Here, the velocity potential is defined as  $\nabla \phi = U_0 + \nabla \phi'$ , where the perturbed velocity is  $\nabla \phi' = \mathbf{u}'$ . Since  $\phi'$  can also be represented by a disturbance of the form  $\phi'(\mathbf{x}, t) = \hat{\phi}(z) e^{ik(x-ct)}$ , the expression for  $\hat{p}$  is found as

$$\hat{p} = \rho \left[ 1 + \frac{\tau_s}{1 + ik\tau(U_0 - c)} \right] [g\hat{a} - ik(U_0 - c)\hat{\phi}]. \quad (18)$$

The boundary conditions are taken at the far field and species interface. First, the velocity potentials in each species are defined as

$$\phi' = \begin{cases} \phi'_2 & z > a \\ \phi'_1 & z < a, \end{cases} \quad (19)$$

Here, subscripts 1 and 2 correspond to the light and heavy gases, respectively. At the far field, the disturbance is zero, so that the following far field conditions are taken:

$$\begin{aligned} \phi'_2(\infty) &= 0, \\ \phi'_1(-\infty) &= 0. \end{aligned} \quad (20)$$

Since  $\Delta\phi'_j=0$  (where the subscript  $j$  indicates the specie 1 or 2),  $\phi'_j$  is found as

$$\begin{aligned} \phi'_2 &= \beta e^{kz}, \\ \phi'_1 &= \alpha e^{-kz}. \end{aligned} \quad (21)$$

Two boundary conditions at the interface are enforced.<sup>14,30</sup> First, the fluid motion at the interface is given as

$$\frac{\partial\phi'_i}{\partial z} = \frac{\partial a}{\partial t} + U_j \frac{\partial a}{\partial x}. \quad (22)$$

From Eqs. (20)–(22),  $\alpha$  and  $\beta$  are found

$$\begin{aligned} \beta &= i(U_2 - c)a, \\ \alpha &= -i(U_1 - c)a. \end{aligned} \quad (23)$$

Also, the pressure at the species interface is continuous (i.e.,  $\widehat{p}_1(a) = \widehat{p}_2(a)$ )

$$\begin{aligned} \hat{p} &= \rho_1 \left[ 1 + \frac{\tau_1 s_1}{1 + ik\tau_1(U_1 - c)} \right] [g\hat{a} - ik(U_1 - c)\widehat{\phi}_1] \\ &= \rho_2 \left[ 1 + \frac{\tau_2 s_2}{1 + ik\tau_2(U_2 - c)} \right] [g\hat{a} - ik(U_2 - c)\widehat{\phi}_2]. \end{aligned} \quad (24)$$

Combining Eqs. (23) and (24), and approximate  $\hat{\phi}$  on the interface by first order (i.e.  $e^{ka} \approx 1.0$ ;  $e^{-ka} \approx 1.0$ )

$$\begin{aligned} \rho_1 \left[ 1 + \frac{\tau_1 s_1}{1 + ik\tau_1(U_1 - c)} \right] [g - k(U_1 - c)^2] \\ = \rho_2 \left[ 1 + \frac{\tau_2 s_2}{1 + ik\tau_2(U_2 - c)} \right] [g + k(U_2 - c)^2] \end{aligned} \quad (25)$$

which is a general expression for instability applicable for KHI, RTI, and RMI. Note that Eq. (25) becomes the same expression derived by Michael<sup>14</sup> if  $\rho_1 = \rho_2$  and  $g=0$ . Since flow in RTI and RMI is initially at rest,  $U_1 = U_2 = 0$  is applicable in Eq. (25), and the following equation is obtained for a two-phase RTI or RMI:

$$\rho_1 \left[ 1 + \frac{f_1}{1 - ik\tau_1 c} \right] (g - kc^2) = \rho_2 \left[ 1 + \frac{f_2}{1 - ik\tau_2 c} \right] (g + kc^2), \quad (26)$$

where  $f_1$  and  $f_2$  are, respectively, the mass loading in light and heavy gases given by  $f_j = mN_0/\rho_j = \tau_j s_j$ . Since the analytical expression presented in Eq. (26) is difficult to solve, the small  $k\tau c$  limit ( $|k\tau c| \ll 1.0$ ) is assumed to simplify Eq. (26) to

$$\rho_1 [1 + f_1] (g - kc^2) = \rho_2 [1 + f_2] (g + kc^2). \quad (27)$$

It might be possible to obtain the solution of Eq. (26) for intermediate and large  $|k\tau c|$  by numerical analysis. However, this study only focuses on small  $|k\tau c|$  limit since the assumption that the mean velocity of the particles is equal to the mean velocity of fluid in Eq. (13) implies that the Stokes number is small, and therefore  $|k\tau c| \ll 1.0$ . A more general formulation will be necessary to develop analytical expressions valid also for intermediate and large  $|k\tau c|$ , and will be revisited in the future.

Then, the wave speed is obtained as

$$c^2 = \frac{g \rho_1 (1 + f_1) - \rho_2 (1 + f_2)}{k \rho_1 (1 + f_1) + \rho_2 (1 + f_2)} = -\frac{g}{k} A_m, \quad (28)$$

where the multiphase Atwood number  $A_m$  is defined as

$$A_m = \frac{\rho_2 (1 + f_2) - \rho_1 (1 + f_1)}{\rho_2 (1 + f_2) + \rho_1 (1 + f_1)}. \quad (29)$$

Note that the real part of  $c$  is found to be zero from Eq. (28), as also seen in the RTI analysis.<sup>30</sup> Equation (29) implies that Atwood number can also be controlled by the particles. Even negative Atwood number that causes inversion of the perturbation<sup>31</sup> is possible if the number density of particle cloud in fluid 1 is large. However, this is not the focus of this paper and we will consider only positive Atwood numbers in this investigation. Also,  $A_m$  becomes identical to the Atwood number used in the original model if there are no particles (i.e.  $f_1 = f_2 = 0$ ). The impulsive model<sup>1</sup> assumes that the fluid interface for RMI is accelerated impulsively as

$$\int g(t) dt = \Delta V. \quad (30)$$

Here, the impulsive model assumes that the particles and the local fluid obtain the same amount of the velocity change  $\Delta V$ . A useful parameter to verify this assumption is the Stokes number  $St$  which is the ratio of the particle response time and the flow time.<sup>32</sup> Here, the flow time scale of RMI is chosen based on the initial growth rate, and  $St$  is defined as

$$St = \frac{\tau}{\tau_{\text{RMI}}}. \quad (31)$$

The time scale for RMI is defined as  $\tau_{\text{RMI}} = a_0/v$ , where  $a_0$  is the initial amplitude of the perturbation and  $v$  is the initial RMI growth rate. When  $St \ll 1.0$ , the particles can catch up with the local velocity very quickly and so that the assumption of the impulsive model is valid, whereas particles do not respond while the RMI is evolving if  $St \gg 1.0$ .<sup>32</sup> The accel-

eration of the interface motion can be described by the following differential equation:<sup>1</sup>

$$\frac{d^2 a(t)}{dt^2} = -a(t)k^2 c^2. \quad (32)$$

If the small  $k\tau c$  assumption is invoked,  $c^2$  in Eq. (32) can be substituted by Eq. (28) resulting in

$$\frac{d^2 a(t)}{dt^2} = a(t)g(t)kA_m. \quad (33)$$

Applying the impulsive model and integrating in time, the following linear growth model for multiphase RMI is obtained:

$$\left. \frac{da(t)}{dt} \right|_{t=0} = -ika_0 = v_{0,m}, \quad (34)$$



FIG. 1. Initial configuration of RMI in a perturbed species interface surrounded by a cloud of solid particles. The grey region denotes the region filled with the gas-particle mixture.

$$a(t) = v_{0,m}t + a_0, \quad (35)$$

where  $v_{0,m} = a_0 k A_m \Delta V$  is the multiphase Richtmyer velocity. Note that if there are no particles ( $f_1 = f_2 = 0$ ), this formulation reduces to the original Richtmyer's model [Eq. (8)]. The wave speed  $c$  is obtained as  $c = -v_{0,m} / (ika_0)$ , so that small  $k\tau c$  limit can be described as

TABLE I. Parameters for the first study and the growth rate obtained from the numerical simulation and theoretical models. Here, Stokes number  $St$  is computed based on the numerically obtained initial growth rate,  $v_{0,num}$ . Thus,  $St_1 = v_{0,num} \tau_1 / a_0$ .

	$r_p$ ( $\mu\text{m}$ )	$f_1$	$f_2$	$\tau_1$ (s)	$\tau_2$ (s)	$\Delta V$	$v_{0,num}$	$A$	$v_0$	$\frac{v_{0,num}}{v_0}$	$A_m$	$v_{0,m}$	$\frac{v_{0,num}}{v_{0,m}}$	$St_1$
No particle		0.0	0.0			68.5	10.46	0.71	12.15	0.86				
Case 0.5-1	0.5	0.88	0.17	$2.09 \times 10^{-6}$	$2.79 \times 10^{-6}$	65	8.00	0.71	11.53	0.69	0.57	9.24	0.87	$4.19 \times 10^{-2}$
Case 0.5-2	0.5	1.75	0.34	$2.09 \times 10^{-6}$	$2.79 \times 10^{-6}$	62	6.28	0.71	10.99	0.57	0.48	7.44	0.84	$3.29 \times 10^{-2}$
Case 0.5-3	0.5	4.34	0.84	$2.09 \times 10^{-6}$	$2.79 \times 10^{-6}$	55	3.53	0.71	9.21	0.38	0.34	4.40	0.80	$1.97 \times 10^{-2}$
Case 0.5-4	0.5	8.69	1.71	$2.09 \times 10^{-6}$	$2.79 \times 10^{-6}$	47	1.88	0.71	7.36	0.26	0.25	2.58	0.73	$1.13 \times 10^{-2}$
Case 1.0-1	1.0	0.70	0.14	$8.37 \times 10^{-6}$	$1.11 \times 10^{-5}$	66	8.82	0.70	11.66	0.76	0.59	9.72	0.91	0.18
Case 1.0-2	1.0	1.41	0.27	$8.37 \times 10^{-6}$	$1.11 \times 10^{-5}$	63	7.33	0.71	11.17	0.66	0.51	8.05	0.91	0.15
Case 1.0-3	1.0	3.53	0.68	$8.37 \times 10^{-6}$	$1.11 \times 10^{-5}$	57	4.27	0.71	10.16	0.42	0.37	5.33	0.80	$8.95 \times 10^{-2}$
Case 1.0-4	1.0	6.95	1.38	$8.37 \times 10^{-6}$	$1.11 \times 10^{-5}$	51	2.31	0.71	8.87	0.26	0.28	3.44	0.67	$4.96 \times 10^{-2}$
Case 2.0-1	2.0	0.61	0.11	$3.35 \times 10^{-5}$	$4.47 \times 10^{-5}$	66	8.90	0.70	12.13	0.73	0.60	10.3	0.86	0.72
Case 2.0-2	2.0	1.21	0.22	$3.35 \times 10^{-5}$	$4.47 \times 10^{-5}$	64	7.48	0.71	12.77	0.59	0.52	9.47	0.79	0.56
Case 2.0-3	2.0	2.94	0.54	$3.35 \times 10^{-5}$	$4.47 \times 10^{-5}$	59	4.51	0.71	12.08	0.37	0.39	6.69	0.67	0.33
Case 2.0-4	2.0	5.65	1.08	$3.35 \times 10^{-5}$	$4.47 \times 10^{-5}$	53	2.38	0.71	10.65	0.22	0.30	4.47	0.53	0.18
Case 4.0-1	4.0	0.52	0.09	$1.34 \times 10^{-4}$	$1.79 \times 10^{-4}$	67	9.45	0.70	11.83	0.80	0.61	10.25	0.92	3.17
Case 4.0-2	4.0	1.04	0.18	$1.34 \times 10^{-4}$	$1.79 \times 10^{-4}$	65	8.42	0.70	11.48	0.73	0.54	8.77	0.96	2.82
Case 4.0-3	4.0	2.51	0.45	$1.34 \times 10^{-4}$	$1.79 \times 10^{-4}$	61	5.60	0.70	10.77	0.52	0.41	6.22	0.90	1.88
Case 4.0-4	4.0	4.57	0.91	$1.34 \times 10^{-4}$	$1.79 \times 10^{-4}$	55	3.68	0.70	9.71	0.38	0.32	4.47	0.82	1.23
Case 8.0-1	8.0	0.22	0.07	$5.36 \times 10^{-4}$	$7.16 \times 10^{-4}$	67	9.94	0.70	11.83	0.84	0.67	11.22	0.89	13.3
Case 8.0-2	8.0	0.44	0.14	$5.36 \times 10^{-4}$	$7.16 \times 10^{-4}$	66	9.31	0.70	11.65	0.80	0.64	10.58	0.88	12.4
Case 8.0-3	8.0	1.13	0.34	$5.36 \times 10^{-4}$	$7.16 \times 10^{-4}$	62	7.96	0.70	10.97	0.73	0.57	8.85	0.90	10.6
Case 8.0-4	8.0	2.27	0.69	$5.36 \times 10^{-4}$	$7.16 \times 10^{-4}$	57	6.46	0.70	10.07	0.64	0.49	7.09	0.91	8.66
Case 16.0-1	16.0	1.99	0.50	$2.14 \times 10^{-3}$	$2.86 \times 10^{-3}$	60	8.65	0.70	10.53	0.82	0.48	7.17	1.21	46.3
Case 16.0-2	16.0	4.04	1.01	$2.14 \times 10^{-3}$	$2.86 \times 10^{-3}$	54	7.11	0.70	9.44	0.75	0.38	5.17	1.38	38.1
Case 16.0-3	16.0	10.33	2.59	$2.14 \times 10^{-3}$	$2.86 \times 10^{-3}$	43	4.84	0.70	7.53	0.64	0.28	3.00	1.61	25.9
Case 16.0-4	16.0	20.90	4.88	$2.14 \times 10^{-3}$	$2.86 \times 10^{-3}$	34	2.77	0.69	5.86	0.47	0.18	1.53	1.80	14.8
Case 32.0-1	32.0	1.97	0.44	$8.58 \times 10^{-3}$	$1.14 \times 10^{-2}$	67	9.76	0.70	11.75	0.83	0.46	7.78	1.25	209
Case 32.0-2	32.0	4.01	0.90	$8.58 \times 10^{-3}$	$1.14 \times 10^{-2}$	65	8.95	0.70	11.39	0.79	0.36	5.86	1.53	191
Case 32.0-3	32.0	10.33	2.30	$8.58 \times 10^{-3}$	$1.14 \times 10^{-2}$	61	7.25	0.69	10.59	0.68	0.23	3.52	2.06	155
Case 32.0-4	32.0	21.41	4.84	$8.58 \times 10^{-3}$	$1.14 \times 10^{-2}$	54	5.51	0.69	9.27	0.59	0.16	2.18	2.52	118
Case 64.0-1	64.0	2.16	0.38	$3.43 \times 10^{-2}$	$4.58 \times 10^{-2}$	67	10.27	0.70	11.81	0.87	0.43	7.18	1.43	881
Case 64.0-2	64.0	4.31	0.76	$3.43 \times 10^{-2}$	$4.58 \times 10^{-2}$	65	9.98	0.70	11.42	0.87	0.30	4.97	2.01	856
Case 64.0-3	64.0	10.97	1.97	$3.43 \times 10^{-2}$	$4.58 \times 10^{-2}$	58	9.01	0.70	10.14	0.89	0.16	2.34	3.86	773
Case 64.0-4	64.0	22.32	4.07	$3.43 \times 10^{-2}$	$4.58 \times 10^{-2}$	56	7.90	0.69	9.74	0.81	0.09	1.24	6.39	677

$$-ik\tau c = \frac{\tau}{a_0/v_{0,m}} = \frac{\tau}{\tau_{\text{RMI}}} = St. \quad (36)$$

Thus, the model indicates that the initial multiphase RMI growth can be described by only two extra parameters for multiphase flow:  $f$  and  $St$ , i.e., particle loading and how soon the particles can respond to the flow.

In summary, the two-phase RMI growth model asymptotes to the classical RMI model in the absence of particles. In the presence of particles, to obtain a modified growth model, following assumptions are necessary:

- (1) Volume fraction of particles is small, so collision effects are neglected (dusty gas formulation);
- (2) The particle shape is spherical and  $Re_d$  is small; thus the drag law is approximated simply by Stokes' law;
- (3)  $St \ll 1.0$  to apply the impulsive model and to simplify Eq. (26).

## IV. RESULTS

We first discuss the case with a shock driven RMI on an air/SF<sub>6</sub> interface surrounded by particles, followed by studies of a shock interaction with a perturbed cloud of solid particles. Since the growth model and the numerical scheme treat the particle phase differently, the numerical setup is chosen to satisfy the assumptions of the dusty gas formulation to enable direct comparisons. Thus, dilute monodispersed particle distribution is used in the present study. For simplicity, we limit ourselves to 2D study here. Full three-dimensional studies will be reported later, but the overall conditions of this study are expected to hold.

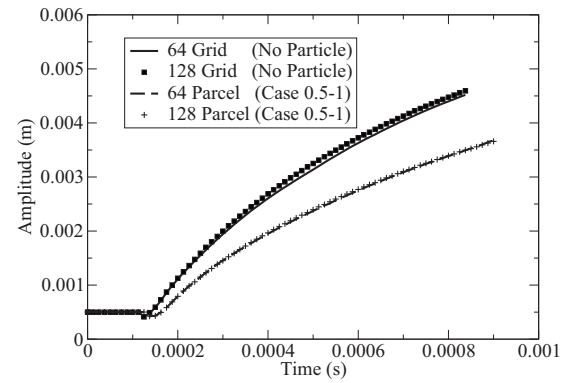
### A. Air/SF<sub>6</sub> interface surrounded by particles

Here, the 2D single-mode air/SF<sub>6</sub> RMI surrounded by a large number of particles is analyzed. The domain configuration used in the current study is shown in Fig. 1; the streamwise length is  $L_x=16$  cm, and the transverse length is  $L_y=1$  cm. The shock, the dusty gas front, and the perturbed species interface are located at 13, 9, and 8 cm, respectively, from the end wall. The incident Mach number is 1.2, and SF<sub>6</sub> and air characterize the initial species interface with a 2D single-mode perturbation as<sup>3</sup>

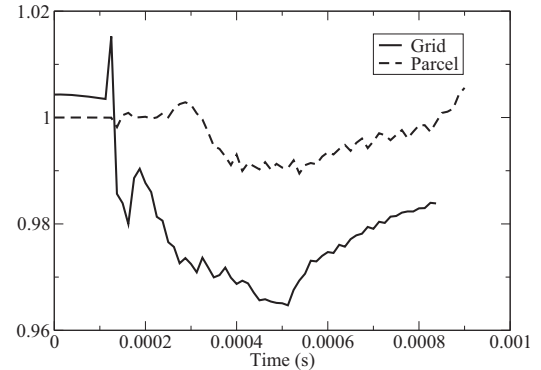
$$a(y) = a_0 \sin\left(\frac{2\pi}{\lambda}y\right) \quad (37)$$

with  $a_0=0.5$  mm and  $\lambda$  is equal to the transverse length of the domain. Spherical particles with a density of 780 kg/m<sup>3</sup> are uniformly distributed along computational cells in the grey region shown in Fig. 1. The amplitude of the perturbation is measured as the half length of the isocontour of the mass fraction at the species interface.<sup>33</sup>

Parametric studies of RMI particle interactions with different values of  $f_1$ ,  $f_2$ ,  $\tau_1$ , and  $\tau_2$  are analyzed by changing the particle sizes and number density. Eight different particle sizes corresponding to four different mass loadings are simulated. The parameters of different cases, the predictions by the original RMI growth model, the multiphase RMI growth model, and the numerical predictions are in Table I. Note that



(a) Growth rate comparisons



(b) Error Analysis

FIG. 2. Comparison of the effect of the assigned number of parcels on the amplitude growth. Here, “64 grid” and “128 grid” correspond to the grid size in the  $y$ -direction. The legend “64 parcel” indicates the case with 64 parcels initialized in the  $y$ -direction (i.e., initially one parcel per cell), and “128 parcel” uses 128 parcels in the  $y$ -direction, with the distance between parcels being half of the 64 parcel case (i.e., 128 corresponds to four parcels per cell initially.)

$\tau$  is computed from the properties after the incident shock passes the interface, and  $f$  is computed by also considering the compression of number density of particles due to the incident shock.

The effects of grid resolution and parcel distribution are presented in Fig. 2. The amplitudes without particles are numerically obtained using two different grid sizes ( $1024 \times 64$  and  $2048 \times 128$ ). For the curve titled “grid” in Fig. 2, there is a slight difference (less than 0.5%) in the amplitude even before the shock hits the perturbation since the number of grid cells to resolve the initial perturbation shape is different for different grid sizes, thereby causing some numerical diffusion. However, these discrepancies are minimal; overall, it is shown that the growth obtained by the coarser grid stays within about 2% in the linear regime [Fig. 2(b)] and has a maximum of 4% at late times. Since we are only interested in the earlier linear regime in this investigation, the  $1024 \times 64$  grid is used for the remainder of this study. Also, the number of parcels required per cell (and the number of particles per parcel to be assigned) has been investigated. For example, two distributions of parcels with the condition of case 0.5-1 are compared, and this represents the baseline case. In one case, 64 parcels in the  $y$ -direction are distributed evenly in the  $x$ -direction; therefore, one parcel is allocated per cell. The other case uses 128 parcels in the  $y$ -direction,

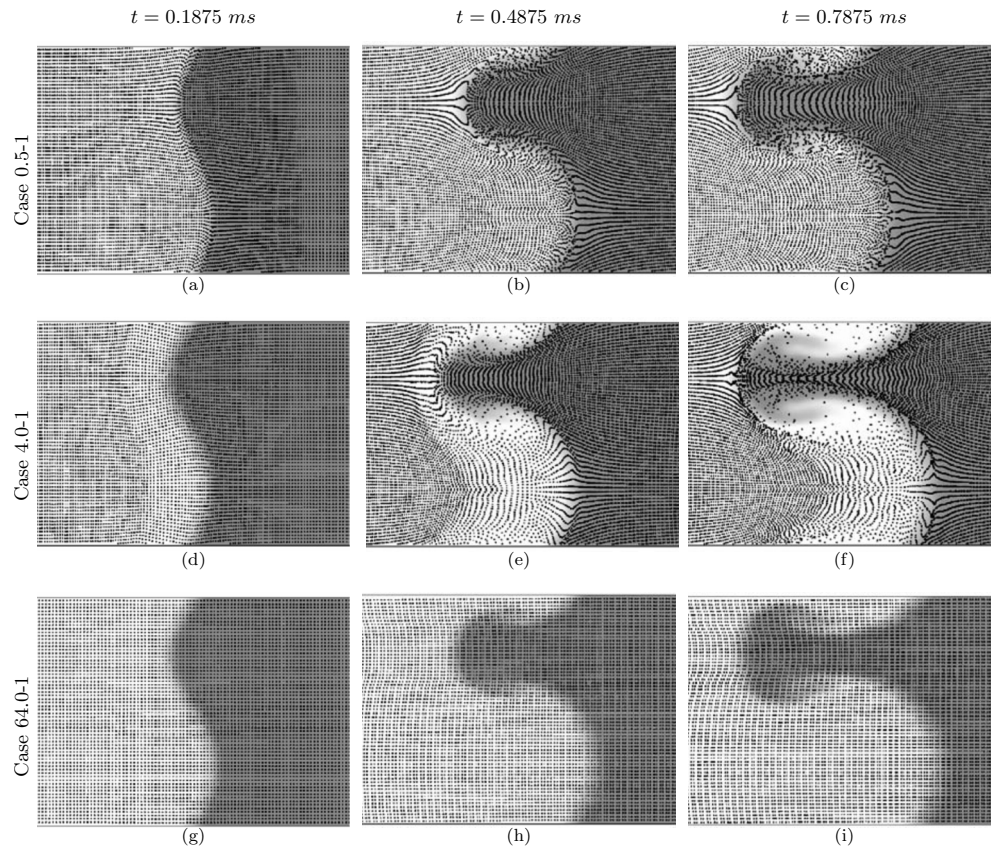


FIG. 3. Contour of mass fraction of  $\text{SF}_6$  with particle distribution (black dots). The first row corresponds to  $St \ll 1.0$  (case 0.5-1), the second row to  $St \approx 1.0$  (case 4.0-1), and the third row to  $St \gg 1.0$  (case 64.0-1).

with equal interparticle spacing maintained also in the  $x$ -direction; this case corresponds to four parcels initially allocated per cell. As evident in Fig. 2(b), both these cases show nearly identical growth rates with an error of only 1%, thereby exemplifying that 64 parcels suffice in the  $y$ -direction for the chosen dimensions. Thus, for the rest of this study, we initialize 64 parcels in the  $y$ -direction, and use the same inter-particle spacing also in the  $x$ -direction.

The flow visualizations of different sizes of particles around RMI interfaces are presented in Fig. 3, with case 0.5-1 in the first row, case 4.0-1 in the second row, and case 64.0-1 in the third row. All the three cases show very different particle distributions at later times, and can be characterized by Stokes number. In general, past studies have shown that particles cluster at regions with low vorticity<sup>34,35</sup> if  $St \approx 1.0$ . On the other hand, if  $St$  is very large, particles do not easily respond to the fluid motion, whereas small  $St$  results in particles following the fluid motion very closely; hence, preferential concentration of particles does not occur in either of these cases.<sup>32</sup> Case 4.0-1 shows that the particles avoid the hydrodynamic roll-ups, and particle clustering is seen in the spikes since the Stokes number for this case is the order of 1.0 ( $St \approx 3.0$ ). However, the case 0.5-1 shows that the particles distribute even within the roll-ups, since Stokes number is very low ( $St \approx 0.04$ ) and the particles inevitably follow the flow. On the other hand, case 64.0-1 shows that the particles barely disperse since the Stokes number is very large ( $St \approx 880$ ). These observations are similar to the findings of

Ling *et al.*,<sup>32</sup> who investigated particle cloud interaction with temporal mixing layers.

In Table I, both single-phase and multiphase RMI growth models are compared with the numerical predictions. The growth rate without particles (denoted as “no particle”) obtained from the numerical simulation,  $v_{0,\text{num}}$  is slightly smaller than the classical Richtmyer velocity  $v_0$  ( $v_{0,\text{num}}/v_0 = 0.86$ ) due to the Richtmyer’s model overpredicting the growth rate, as also reported by Latini *et al.*<sup>6</sup> The numerical prediction of case 0.5- $X$  (where  $X$  denotes 1, 2, 3, and 4) shows good agreement with the multiphase Richtmyer velocity [Eq. (35)] since the particle response time is very small and the model assumptions are valid (e.g.  $St \ll 1.0$ ).

The growth rate of the series of case 0.5- $X$  and the no particle cases are examined in Fig. 4. As the particle loading increases, the initial growth rate decreases since both  $A_m$  and  $\Delta V$  decrease as the mass loading increases. In Fig. 5, the same amplitude is normalized and presented (note that the multiphase Richtmyer velocity is used). The normalized growth rate shows good agreement in the early stage; for example, case 0.5-1 follows nearly exactly up to  $kv_{0,m}t < 1$ , but starts to depart from the no particle case eventually (Fig. 5). The reason for the different late-time growth may be the nonuniform distributions of particles, which occur when the perturbations grow larger at late times. Due to the nonuniform distribution of particles around the hydrodynamic structures as shown in Fig. 3, the late-time growth rate of the perturbation will be different from the no particle case. It

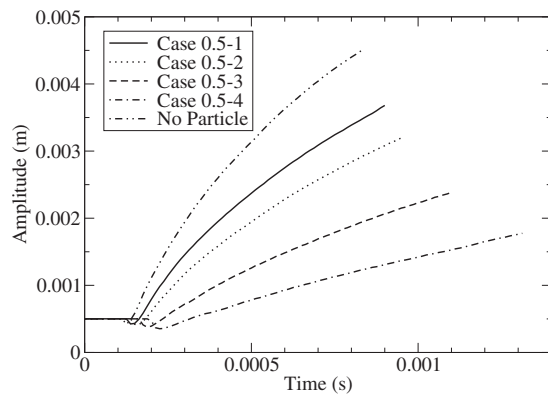


FIG. 4. Amplitude growth for small particles with different loading (case 0.5- $X$ ) and the no particle case.

might be interesting to extend the definition of  $A_m$  to nonlinear growth models that have been developed in the past<sup>36,37</sup> for the single-phase RMI to predict the growth rates for multiphase flow fields as well. The comparisons have not been made since the normalized initial amplitude growth rates ( $\frac{v_{0,num}}{v_{0,m}}$ ) in each case 0.5- $X$  is different as shown in Fig. 5, whereas the normalized initial amplitude growth rates should not be a function of Atwood number in a single-phase RMI. We believe that the simple extension of  $A$  to  $A_m$  would not work since these models are established upon the assumption of incompressibility, but as seen in Fig. 3, lateral particle dispersion and clustering are observed for case 0.5- $X$  even when the Stokes number is very small. Therefore, more comprehensive models that can also account for particle dispersions and response times would be necessary to model nonlinear regimes. Further investigation along these lines is necessary to investigate RMIs in gas-particle mixtures.

The multiphase RMI model also shows a better prediction than the original Richtmyer model up to case 8.0- $X$  ( $r_p \leq 8.0 \mu\text{m}$ ). It is unexpected to see that case 4.0- $X$  and case 8.0- $X$  follow the multiphase RMI model well since  $St > 1.0$  for these cases and the assumptions of the multiphase RMI are not valid. However, numerical predictions show very good agreement with the multiphase RMI model. It could presumably be due to nonlinear fluid-particle interac-

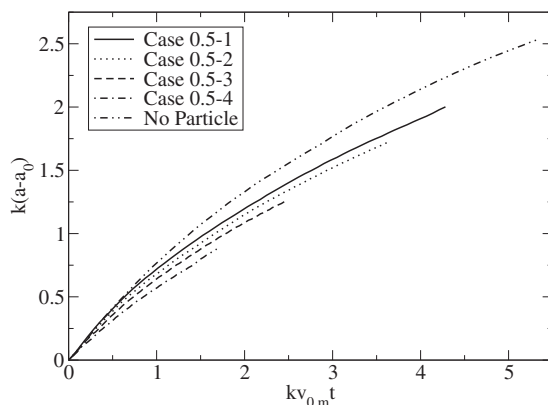


FIG. 5. Normalized amplitudes for case 0.5- $X$  and the no particle cases. The  $x$ -axis is normalized by the multiphase Richtmyer velocity.

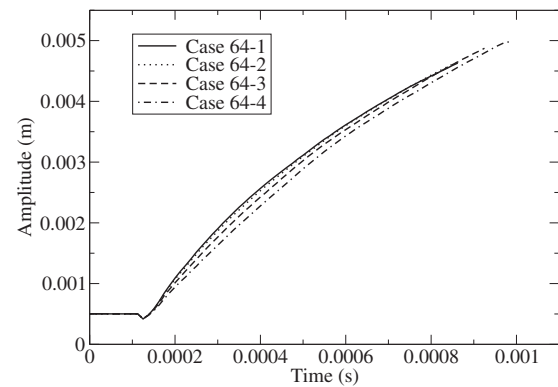


FIG. 6. Amplitude growth for large particles with different loading (case 64.0- $X$ ).

tions, but more general theoretical models could be developed in the future to explain the phenomena more precisely. However, for much larger particles ( $r_p \geq 16.0 \mu\text{m}$ ,  $St \gg 1.0$ ) the two-phase model is inapplicable, and the original Richtmyer velocity shows better predictions. This makes sense since the original RMI is for single-phase flow. In fact, case 64.0- $X$  follows the original Richtmyer velocity very closely since the particles are not significantly influenced during the RMI growth process. Owing to their higher inertia, these particles have  $St \approx 800$ . Furthermore, changing the mass loading does not influence the growth rate as much as the small particle cases shown in Fig. 6, since interphase momentum exchange is not very significant. The growth profiles normalized by the original Richtmyer velocity are nearly identical up to  $kv_0t = 2.0$  including the no particle case as shown in Fig. 7, indicating that the presence of particles does not influence the perturbation growth when  $St \gg 1.0$ .

In summary, results for a RMI surrounded by a uniform distribution of particles suggest that when the particle response time is relatively small ( $St \ll 1.0$ ), the growth rates agree very well with the multiphase Richtmyer velocity. However, when the particle response time is very large ( $St \gg 1.0$ ), the particles are not influenced by the fluid, and the amplitude growth follows the original Richtmyer velocity. Thus, the particle response time is a very important factor to control the applicability of both the current multiphase

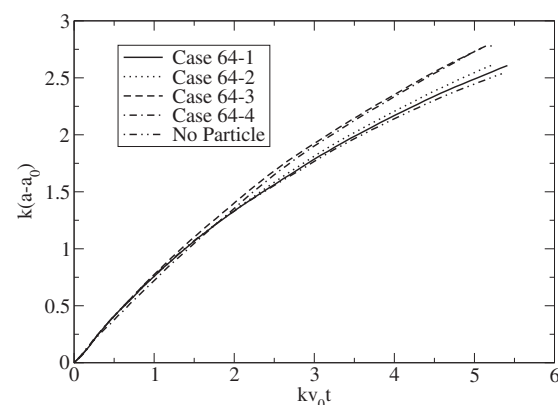


FIG. 7. Normalized amplitudes for case 64.0- $X$  and the no particle cases. The  $x$ -axis is normalized by the single phase Richtmyer velocity.



FIG. 8. Initial configuration of RMI of the perturbed shape particle clouds. The grey region denotes the region filled with the gas-particle mixture.

growth model as well as the original Richtmyer's growth model. In the next section, the second RMI problem involving the perturbed shape particle cloud in air is analyzed.

## B. Perturbed shape particle cloud

In this section, the RMI is investigated for a shock wave interaction with a cloud of solid particles with a perturbed shape in air instead of a heavy gas (such as  $\text{SF}_6$ ). A schematic of the setup is presented in Fig. 8. The dusty gas front and the shock front are placed 8 and 9 cm from the end wall, respectively, and the initial amplitude of the perturbation of the dusty gas is 0.5 mm. The same domain size ( $16 \times 1$  cm) and grid resolution ( $1024 \times 64$ ) of the first study are used here. The incident Mach number is 1.2 as well, and the domain is filled with air only. The amplitude of the perturbed particle cloud is defined as half of the length of the dispersion in the  $x$ -direction of the particles that are initially placed in the front row. Five different particle sizes with four different mass loadings are studied, and Table II summarizes the parameters and the results of each case. Here, the multiphase RMI growth model and numerical predictions are compared.

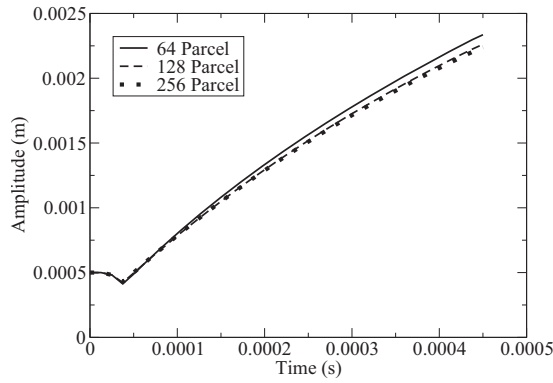
In order to ascertain the choice of the number of parcels to represent the particle cloud for the simulations, three different parcel distributions are simulated for case P0.5-1 and presented in Fig. 9. The case with 64 parcels slightly overpredicts the growth at late times by about 4% whereas 128 and 256 parcel cases show very good agreement with only about 1% error. Thus, 128 parcels in the  $y$ -directions are used for the rest of this section.

Figure 10 compares the evolution of the perturbation of a particle cloud for different Stokes numbers, for the cases P0.5-4 and P2.0-4. For case P0.5-4, narrow spikes are observed and the particles undergo less transverse dispersion *vis-à-vis* the P2.0-4 case; due to this, the particle cloud interfaces are sharper for P0.5-4. However, case P2.0-4 shows wider spikes that result in the dispersion of particles around the spike at late times, clearly demonstrating that different particle dispersion is due to differences in the Stokes number. As Uchiyama and Yagami<sup>38</sup> pointed out, when a vortex ring interacts with a particle cloud, it can cause particles to move outside the vortex ring due to a centrifugal force. As a result, the particles are distributed over a wider region around the vortex ring. However, the Stokes number for the particles in case P0.5-4 is very small,  $St \approx 0.04$ , due to which the particles follow the fluid motion rather than being dispersed by the vortex rings.

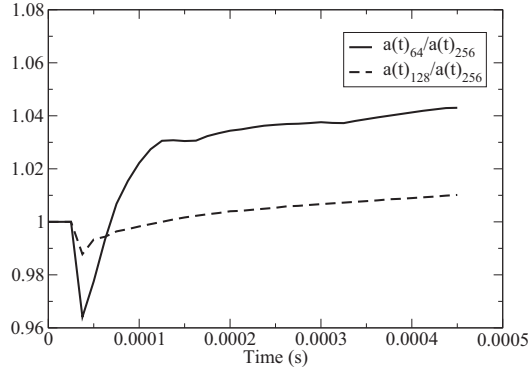
The numerical prediction of the growth rate of small particles cases (case P0.5- $X$  and case P1.0- $X$ ) are close to the multiphase RMI model ( $v_{0,\text{num}}/v_{0,m} \approx 0.8$ ) as seen in the previous section (Table I). The growth of the dusty gas perturbation is shown in Fig. 11; unlike the earlier result, the cases corresponding to a higher mass loading tend to have higher

TABLE II. Parameters and results for the second kind of multiphase RMI. The results of cases P4.0- $X$  and P8.0- $X$  are not listed because the acceleration of the particles for these cases is not impulsive due to the high inertia of the particles, and  $\Delta V$  could not be determined for the same reason.

	$r_p$ ( $\mu\text{m}$ )	$f_2$	$\tau_2$ (s)	$\Delta V$	$v_{0,\text{num}}$	$A_m$	$v_{0,m}$	$\frac{v_{0,\text{num}}}{v_{0,m}}$	$St_2$
Case P0.5-1	0.5	0.86	$2.05 \times 10^{-6}$	88	5.81	0.30	6.71	0.84	$2.90 \times 10^{-2}$
Case P0.5-2	0.5	1.77	$2.05 \times 10^{-6}$	78	8.13	0.46	9.21	0.80	$3.78 \times 10^{-2}$
Case P0.5-3	0.5	4.37	$2.05 \times 10^{-6}$	62	9.44	0.68	10.84	0.75	$4.13 \times 10^{-2}$
Case P0.5-4	0.5	8.73	$2.05 \times 10^{-6}$	50	9.85	0.81	10.41	0.79	$4.18 \times 10^{-2}$
Case P1.0-1	1.0	0.69	$8.22 \times 10^{-6}$	90	4.77	0.25	5.82	0.80	$9.52 \times 10^{-2}$
Case P1.0-2	1.0	1.41	$8.22 \times 10^{-6}$	81	6.98	0.40	8.36	0.79	0.134
Case P1.0-3	1.0	3.47	$8.22 \times 10^{-6}$	66	9.44	0.63	10.65	0.79	0.172
Case P1.0-4	1.0	6.94	$8.22 \times 10^{-6}$	53.5	10.02	0.77	10.61	0.81	0.175
Case P2.0-1	2.0	0.56	$3.28 \times 10^{-5}$	92	3.1	0.21	5.03	0.62	0.253
Case P2.0-2	2.0	1.12	$3.28 \times 10^{-5}$	84	4.75	0.35	7.52	0.63	0.388
Case P2.0-3	2.0	2.78	$3.28 \times 10^{-5}$	70	7.59	0.57	10.32	0.74	0.621
Case P2.0-4	2.0	5.55	$3.28 \times 10^{-5}$	57.5	9.08	0.73	10.78	0.84	0.743
Case P4.0-1	4.0	0.35	$1.31 \times 10^{-4}$						
Case P4.0-2	4.0	0.89	$1.31 \times 10^{-4}$						
Case P4.0-3	4.0	2.31	$1.31 \times 10^{-4}$						
Case P4.0-4	4.0	4.47	$1.31 \times 10^{-4}$						
Case P8.0-1	8.0	1.03	$5.26 \times 10^{-4}$						
Case P8.0-2	8.0	2.04	$5.26 \times 10^{-4}$						
Case P8.0-3	8.0	2.94	$5.26 \times 10^{-4}$						
Case P8.0-4	8.0	3.82	$5.26 \times 10^{-4}$						



(a)Growth Rate comparisons



(b)Error Analysis

FIG. 9. Comparison of the effect of number of parcels to the amplitude growth for the second kind of RMI under study for case P0.5-1. In the legend, 64 parcel, 128 parcel, and 256 parcel denote the number of parcels used in the  $y$ -direction, respectively, with the corresponding interparcel distance applied also in the  $x$ -direction.

growth rates since it generates a higher  $A_m$ . However, a higher mass loading leads to slower  $\Delta V$ , and therefore results in smaller  $v_{0,m}$ . In fact, from Table II, the model prediction of  $v_{0,m}$  in case P0.5-3 is larger than case P0.5-4 even though the numerical results are opposite. The normalized growth rates indicate that the growth of the dusty gas perturbation is even comparable to the single-phase RMI, especially up to  $kv_0t$

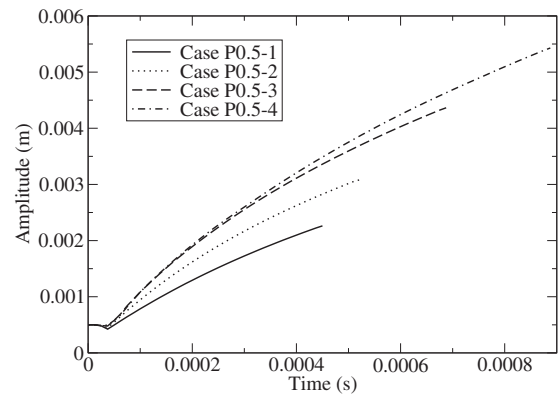


FIG. 11. Amplitude growth of perturbed shape particle clouds with different initial particle mass loadings for case P0.5- $X$  ( $X=1, 2, 3,$  and  $4$ ).

$< 2.0$ , as presented in Fig. 12. Thus, the results indicate that the dispersion of perturbed shape particle clouds can be explained by multiphase RMI growth models, even though it is hitherto not treated as a RMI problem in literature.

However, the growth of the perturbation follows RMI only for small  $St$ . If larger particles are used, they rather experience continuous acceleration until the particles and the gas attain equilibrium (in terms of velocity). Therefore, the amplitude growth rate of the heavier particle accelerates in the initial stage as presented in Fig. 13, and shows exponential growth instead of linear growth as seen in the RTI at early times.<sup>36</sup>

In summary, the amplitude growth of perturbed shape particle cloud in air is investigated for a range of conditions by using numerical simulations and compared with the developed multiphase RMI model. The results show that the growth rates of the simulations are predicted well by the multiphase RMI growth model, and the normalized amplitude growth rates are in accordance with the gas phase RMI. Therefore, this study suggests that dilute particle cloud dispersion by a shock wave can be treated as a RMI as long as the particle response time is small. However, if the particle

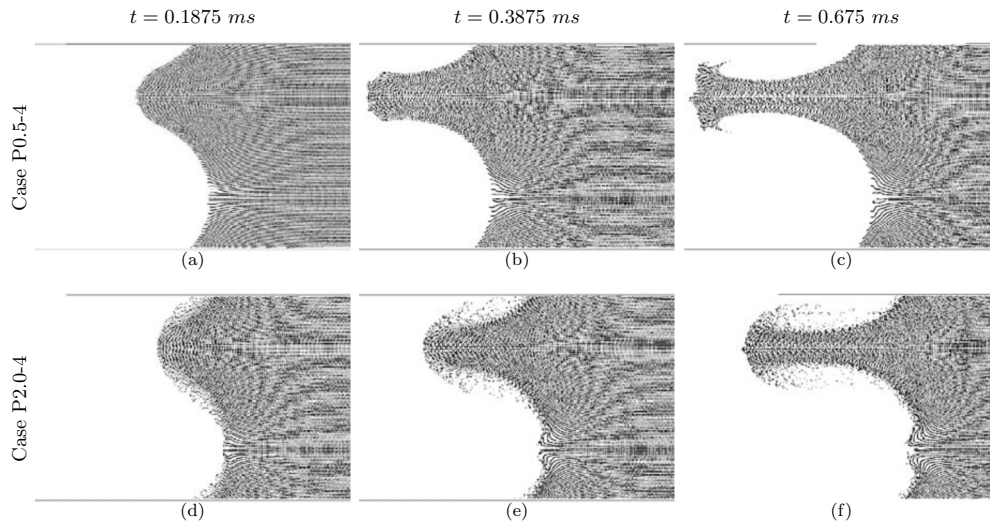


FIG. 10. Particle distribution around the RMI structure at different times for the second kind of RMI.

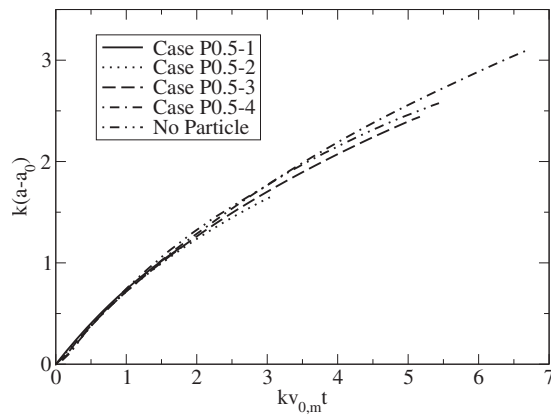


FIG. 12. Normalized amplitude of perturbed shape particle clouds for cases P0.5- $X$  ( $X=1, 2, 3,$  and  $4$ ).

response time is large, the particles experience continuous acceleration, and the growth of the interface shows exponential growth similar to RTI.

## V. CONCLUSIONS

The present study derives the growth model of multiphase RMI by using dusty gas assumptions, and analyzes two kinds of RMIs in gas-particle mixtures. For a RMI involving an air/SF<sub>6</sub> interface surrounded by a uniformly distributed particle cloud, it is found that the multiphase RMI model predicts the numerical simulation growth rates better than the original RMI model when the particle response time,  $St < 10.0$ . However, when the particle response time is larger, the growth rates follow the original Richtmyer's model since the particles do not follow the fluid motion and the RMI process is entirely based on the gas phase. When the Stokes number is on the order of unity, preferential concentration of particles is found. However, when the Stokes number is small ( $St \approx 0.04$ ), relatively uniform particle distribution is observed in the high vorticity region. For large Stokes number ( $St \approx 880$ ), on the other hand, the particles are not influenced by the fluid motion. The second type of multiphase RMI involves the multiphase growth of the perturbed particle cloud by a shock wave. Here, too, the multiphase RMI growth model shows good agreement with the numeri-

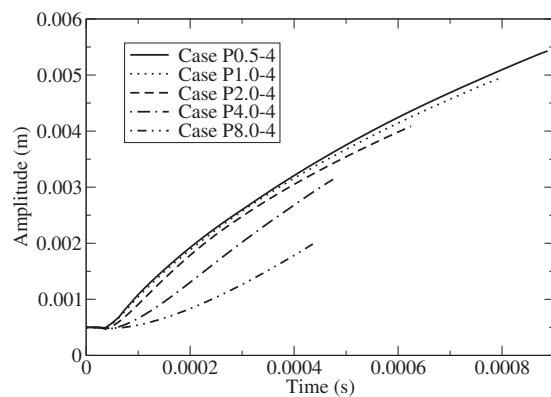


FIG. 13. Changes in the behavior of the amplitude growth for different particle sizes.

cal results, and the normalized growth rate of each case corresponds to the single-phase RMI even at late times. However, requirements on the particle response time is stricter, and the impulsive acceleration is found only when  $St \ll 1.0$ . If the particles response time is large, particles experience continuous acceleration after the shock, which results in a RTI-like exponential growth rate at early times.

## ACKNOWLEDGMENTS

This work is supported by the Defense Threat Reduction Agency (Dr. S. Peiris, program manager) The computational resources were provided by the Department of Defense High Performance Computing Centers at ERDC, NAVO, and ARL.

- <sup>1</sup>R. D. Richtmyer, "Taylor instability in shock acceleration of compressible fluids," *Commun. Pure Appl. Math.* **13**, 297 (1960).
- <sup>2</sup>J. D. Meshkov, "Instability of the interface of two gases accelerated by shock wave," *Fluid Dyn.* **4**, 101 (1969).
- <sup>3</sup>B. D. Collins and J. W. Jacobs, "PLIF flow visualization and measurements of the Richtmyer–Meshkov instability of an air/SF<sub>6</sub> interface," *J. Fluid Mech.* **464**, 113 (2002).
- <sup>4</sup>J. W. Jacobs and V. V. Krivets, "Experiments on the late-time development of single-mode Richtmyer–Meshkov instability," *Phys. Fluids* **17**, 034105 (2005).
- <sup>5</sup>P. R. Chapman and J. W. Jacobs, "Experiments on the three-dimensional incompressible Richtmyer–Meshkov instability," *Phys. Fluids* **18**, 074101 (2006).
- <sup>6</sup>M. Latini, O. Schilling, and W. S. Don, "High-resolution simulations and modeling of reshocked single-mode Richtmyer–Meshkov instability: Comparison to experimental data and to amplitude growth model predictions," *Phys. Fluids* **19**, 024104 (2007).
- <sup>7</sup>U. Alon, J. Hecht, D. Ofer, and D. Shvarts, "Power laws and similarity of Rayleigh–Taylor and Richtmyer–Meshkov mixing fronts at all density ratio," *Phys. Rev. Lett.* **74**, 534 (1995).
- <sup>8</sup>M. Vetter and B. Sturtevant, "Experiments on the Richtmyer–Meshkov instability," *Shock Waves* **4**, 247 (1995).
- <sup>9</sup>E. Leinov, G. Malamud, Y. Elbaz, L. A. Levin, G. Ben-Dor, D. Shvarts, and O. Sadot, "Experimental and numerical investigation of the Richtmyer–Meshkov instability under reshock conditions," *J. Fluid Mech.* **626**, 449 (2009).
- <sup>10</sup>M. Lombardini and D. I. Pullin, "Small-amplitude perturbations in the three-dimensional cylindrical Richtmyer–Meshkov instability," *Phys. Fluids* **21**, 114103 (2009).
- <sup>11</sup>K. Balakrishnan and S. Menon, "On the role of ambient reactive particles in the mixing and afterburn behind explosive blast waves," *Combust. Sci. Technol.* **182**, 186 (2010).
- <sup>12</sup>J. N. Cuzzi, R. C. Hogan, J. M. Paque, and A. R. Dobrovolskis, "Size-selective concentration of chondrules and other small particles in protoplanetary nebula turbulence," *Astrophys. J.* **546**, 496 (2001).
- <sup>13</sup>P. G. Saffman, "On the stability of laminar flow of a dusty gas," *J. Fluid Mech.* **13**, 120 (1962).
- <sup>14</sup>D. H. Michael, "Kelvin–Helmholtz instability of a dusty gas," *Proc. Cambridge Philos. Soc.* **61**, 569 (1965).
- <sup>15</sup>D. H. Michael, "The stability of plane Poiseuille flow of a dusty gas," *J. Fluid Mech.* **18**, 19 (1964).
- <sup>16</sup>V. M. Boiko, V. P. Kiselev, S. P. Kiselev, A. N. Papyrin, S. V. Poplavsky, and V. M. Fomin, "Shock wave interaction with a cloud of particles," *Shock Waves* **7**, 275 (1997).
- <sup>17</sup>V. P. Kiselev, S. P. Kiselev, and E. V. Vorozhtsov, "Interaction of a shock wave with a particle cloud of finite size," *Shock Waves* **16**, 53 (2006).
- <sup>18</sup>S. P. Kiselev, E. V. Vorozhtsov, and V. M. Fomin, *Foundations of Fluid Mechanics with Applications* (Birkhäuser, Boston, MA, 1999).
- <sup>19</sup>O. A. Ota, C. J. Barton, and D. A. Holder, "Shock tube experiment: Half-height dense gas region," *Phys. Scr.* **T132**, 014015 (2008).
- <sup>20</sup>D. M. Snider, "An incompressible three-dimensional multiphase particle-in-cell model for dense particle flows," *J. Comput. Phys.* **170**, 523 (2001).
- <sup>21</sup>N. A. Patankar and D. D. Joseph, "Lagrangian numerical simulation of particle flows," *Int. J. Multiphase Flow* **27**, 1685 (2001).

- <sup>22</sup>F. Génin and S. Menon, "Studies of shock/turbulent shear layer interaction using large-eddy simulation," *Comput. Fluids* **39**, 800 (2010).
- <sup>23</sup>F. Génin and S. Menon, "Simulation of turbulent mixing behind a strut injector in supersonic flow," *AIAA J.* **48**, 526 (2010).
- <sup>24</sup>F. Génin and S. Menon, "Dynamics of sonic jet injection into supersonic crossflow," *J. Turbul.* **11**, N4 (2010).
- <sup>25</sup>S. Menon and N. Patel, "Subgrid modeling for simulation of spray combustion in large-scale combustors," *AIAA J.* **44**, 709 (2006).
- <sup>26</sup>C. Crowe, M. Sommerfeld, and Y. Tsuji, *Multiphase Flows with Droplets and Particles* (CRC, Boca Raton, 1998).
- <sup>27</sup>M. R. Maxey and J. J. Riley, "Equation of motion for a small rigid sphere in a nonuniform flow," *Phys. Fluids* **26**, 883 (1983).
- <sup>28</sup>S. I. Pai, S. Menon, and Z. Q. Fan, "Similarity solutions of a strong shock wave propagation in a mixture of a gas and dusty particles," *Int. J. Eng. Sci.* **18**, 1365 (1980).
- <sup>29</sup>E. Loth, "Numerical approaches for motion of dispersed particles, droplets, and bubbles," *Prog. Energy Combust. Sci.* **26**, 161 (2000).
- <sup>30</sup>P. G. Drazin, *Introduction to Hydrodynamic Stability* (Cambridge Texts Applied Mathematics, Cambridge, UK, 2002).
- <sup>31</sup>N. J. Zabusky, "Vortex paradigm for accelerated inhomogeneous flows: Visiometrics for the Rayleigh–Taylor and Richtmyer–Meshkov environments," *Annu. Rev. Fluid Mech.* **31**, 495 (1999).
- <sup>32</sup>W. Ling, J. N. Chung, T. R. Troutt, and C. T. Crowe, "Direct numerical simulation of a three-dimensional temporal mixing layer with particle dispersion," *J. Fluid Mech.* **358**, 61 (1998).
- <sup>33</sup>M. Brouillette and B. Sturtevant, "Experiments on the Richtmyer–Meshkov instability: Single-scale perturbations on a continuous interface," *J. Fluid Mech.* **263**, 271 (1994).
- <sup>34</sup>J. R. Fessler, J. D. Kulick, and J. K. Eaton, "Preferential concentration of heavy particles in a turbulent channel flow," *Phys. Fluids* **6**, 3742 (1994).
- <sup>35</sup>O. Simonin, P. Février, and J. Laviéville, "On the spatial distribution of heavy-particle velocities in turbulent flow: From continuous field to particulate chaos," *J. Turbul.* **3**, 40 (2002).
- <sup>36</sup>K. O. Mikaelian, "Explicit expressions for the evolution of single mode Rayleigh–Taylor and Richtmyer–Meshkov instabilities at arbitrary Atwood numbers," *Phys. Rev. E* **67**, 026319 (2003).
- <sup>37</sup>O. Sadot, L. Erez, U. Alon, D. Oron, L. A. Levin, G. Erez, D. Shvarts, and G. Ben-Dor, "Study of nonlinear evolution of single-mode and two-bubble interaction under Richtmyer–Mesukov instability," *Phys. Rev. Lett.* **80**, 1654 (1998).
- <sup>38</sup>T. Uchiyama and H. Yagami, "Numerical simulation for the collision between a vortex ring and solid particles," *Powder Technol.* **188**, 73 (2008).